


Spin-driven ferroelectricity in the quantum magnet TlCuCl_3 under high pressureKyosuke Sakurai, Shojiro Kimura ^{*} and Staoshi Awaji*Institute for Materials Research, Tohoku University, Katahira 2-1-1, Sendai 980-8577, Japan*Masashige Matsumoto *Department of Physics, Shizuoka University, Shizuoka 422-8529, Japan*Hidekazu Tanaka *Department of Physics, Tokyo Institute of Technology, Tokyo 152-8551, Japan*

(Received 11 May 2020; revised 27 July 2020; accepted 29 July 2020; published 14 August 2020)

In this study, dielectric constant and pyroelectric current measurements under high pressure up to 16.7 kbar have been performed for the interacting spin dimer system TlCuCl_3 , which exhibits spin-driven ferroelectricity in the magnon Bose-Einstein condensation (BEC) phase with strong quantum spin fluctuation. When pressure is applied, the magnon BEC phase becomes significantly stabilized, whereas the value of the electric polarization decreases in high-pressure regions. It is also observed that electric polarization becomes harder under pressure. Analyses based on both a Landau theory and a microscopic spin Hamiltonian demonstrate that the suppression of quantum fluctuation on the application of pressure caused the observed pressure effects. Consequently, it is revealed that the ferroelectricity in TlCuCl_3 is highly governed by the quantum spin fluctuation.

DOI: [10.1103/PhysRevB.102.064104](https://doi.org/10.1103/PhysRevB.102.064104)**I. INTRODUCTION**

Since the discovery of spin-driven ferroelectricity, wherein the breaking of space inversion symmetry by magnetic order induces ferroelectricity, magnetoelectric (ME) multiferroic materials with both magnetic and ferroelectric order have garnered significant attention [1]. Several spiral magnets and antiferromagnets have been found to exhibit spontaneous electric polarization through magnetic ordering with a polar symmetry [2–4]. The spin-dependent electric dipole moment is a microscopic element that induces coupling between magnetism and electric polarization in spin-driven ferroelectricity. It is expressed using the quadratic terms of spin operators [4–6]. For instance, an electric dipole, which depends on an outer product of two neighboring spins $\mathbf{S}_i \times \mathbf{S}_j$ (called vector spin chirality), causes ferroelectricity via the cycloidal magnetic order [4,7–11]. It is noteworthy that because the expected value of a spin-dependent electric dipole is given by a form of two spin correlation functions, not only an ordered spin component but also quantum fluctuation—in other words, quantum entanglement—of spins can contribute to the spontaneous electric polarization in ME multiferroics, as will be discussed in the following sections. However, there is a lack of studies on the effect of quantum fluctuation on ME multiferroics [12,13], because spin-driven ferroelectricity has mostly been observed in classical magnets thus far. The interacting spin dimer system TlCuCl_3 is the best compound to investigate this quantum-mechanical aspect of ME multiferroics. This compound was reported to exhibit ferroelectricity

in its magnetic-field-induced magnon Bose-Einstein condensation (BEC) phase [14–16], in which strong quantum spin fluctuation is involved.

In TlCuCl_3 , $S = 1/2$ antiferromagnetic dimers, composed of two Cu^{2+} , are coupled by relatively weak interdimer interactions, forming a three-dimensional (3D) network [17]. This compound remains a quantum paramagnet even in the lowest temperature due to its spin-singlet ground state at zero magnetic field [18]. However, in an external magnetic field, a bosonic quasiparticle called a magnon, which is an excited triplet on a dimer propagating through the network, is condensed into the ground state above the critical field $H_0 \simeq 5.5$ T where the energy gap of the magnon is closed by the field. Therefore, TlCuCl_3 undergoes antiferromagnetic ordering due to the magnon BEC for $H > H_0$ [19–23]. The magnetic order is a two-sublattice type with antiparallel alignment of the transverse components of spins on a dimer [24]. The quantum fluctuation inherent in the dimer structure largely suppresses the magnitude of the ordered magnetic moment to approximately 30% of a full moment of Cu^{2+} even at 12 T, which is significantly greater than H_0 . This magnon BEC leads not only to antiferromagnetic order but also to ferroelectricity [14,15]. This is because the coherent superposition of the singlet and triplet states on a dimer, realized in the BEC phase, has a finite expectation value for the vector spin chirality $\langle \mathbf{S}_l \times \mathbf{S}_r \rangle$ on a dimer with spins \mathbf{S}_l and \mathbf{S}_r . The resulting ferroelectricity is very soft with the lowest cohesive electric field among those of the known ME multiferroics. This soft nature enables us to realize the fast switching of the nonreciprocal directional microwave response by electric fields in TlCuCl_3 [16]. Another important feature of TlCuCl_3 is that its exchange interactions are highly susceptible to the applied pressure.

^{*}shkimura@imr.tohoku.ac.jp

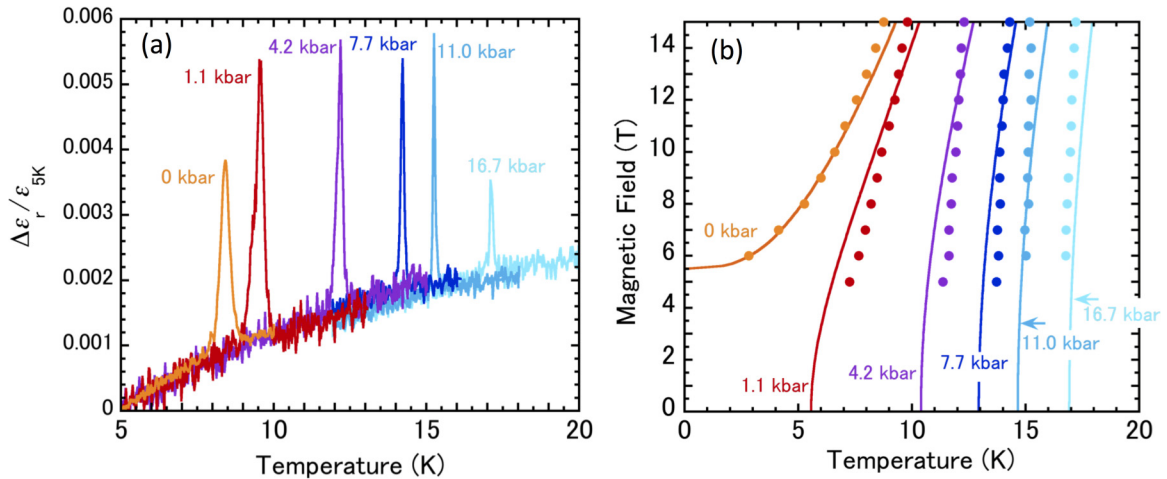


FIG. 1. (a) Temperature dependence of relative change in the dielectric constants under applied pressure, observed in TiCuCl_3 for $H \parallel [201]$ at 14 T. (b) Temperature vs magnetic field phase diagram in TiCuCl_3 . Solid curves represent the theoretical curves, calculated based on the Landau theory.

Lattice deformation due to the application of hydrostatic pressure strengthens the interdimer interactions while weakening the intradimer one. Consequently, the critical field decreases as pressure increases; subsequently, for pressure values above $p \simeq 0.4$ kbar, TiCuCl_3 becomes ordered even in the absence of the external magnetic field [25,26]. The application of pressure relaxes the quantum fluctuation stemming from the dimer nature of TiCuCl_3 , and causes a crossover to a classical 3D antiferromagnet, thereby facilitating the magnetic order. Thus, the application of pressure allows us to tune the strength of the quantum spin fluctuation in TiCuCl_3 . In this study, by measuring the dielectric constant and pyroelectric current under hydrostatic pressure, we demonstrate that the applied pressure considerably affects the phase diagram, the value of electric polarization, and the cohesive field of spin-driven ferroelectricity in TiCuCl_3 via changes in the exchange interactions caused by pressure. The results of our analyses reveal that the quantum fluctuation is essential for determining the nature of the ferroelectricity in TiCuCl_3 .

II. EXPERIMENT

The dielectric constant and pyroelectric current of TiCuCl_3 were measured under high pressure up to 16.7 kbar and in magnetic fields up to 18 T using a superconducting magnet. A two-section piston cylinder pressure cell (C&T Factory Co., Ltd.), made from NiCrAr (inner cylinder) and CuBe (outer sleeve), was used. A platelike crystal was immersed in a Teflon cup filled with Daphne 7474 oil (Idemitsu Kosan Co, Ltd.) as the pressure medium. A single crystal TiCuCl_3 , grown by the Bridgman method, was cut into thin plates with the widest plane parallel to the cleavage $(10\bar{2})$ plane; subsequently, a silver paste was applied on the faces of the crystal as electrodes. The external magnetic field was applied along the $[201]$ axis. We measured the dielectric constant at 10 kHz using an LCR meter (Agilent E4980A). To determine the temperature dependence of the spontaneous electric polarization P , the pyroelectric current was measured after

applying a poling electric field of 0.043 MV/m from the paramagnetic phase using an electrometer (Keithley 6517B). The value of P observed at ambient pressure in this study was smaller than those observed in previous studies [14,15]; this difference occurred because a different sample batch was used in this study. The P - E hysteresis curve was obtained by measuring the displacement current induced by the sweeping electric field E .

III. RESULTS AND DISCUSSION

Figure 1(a) shows the temperature T dependence of the relative changes in the dielectric constant ϵ_r to that at 5 K in TiCuCl_3 observed in the magnetic field $H = 14$ T along the $[201]$ axis under the applied pressure p . Because the antiferromagnetic order is stabilized by the applied pressure, the peak of ϵ_r , which is indicative of the magnetic ordering with the ferroelectricity, shifts toward higher temperature as the pressure is increased. The field-temperature phase diagram obtained from the peak of ϵ_r under pressure is shown in Fig. 1(b). The phase boundary between the paramagnetic and the antiferromagnetic ordered phases moves toward higher temperatures with increasing pressure, thereby demonstrating that the ordered phase is considerably expanded by applied pressure. The convex phase boundary at ambient pressure, which is expressed by $H - H_0 \propto T^\phi$ with a certain coefficient $\phi > 1$ characteristic of the magnon BEC [19,20,23], gradually changes to a concave curve by the application of pressure. From the several types of theoretical approaches to investigate the pressure and magnetic field dependencies of the phase boundary in a spin-gap system [27,28], we adopted the Landau theory to examine the observed behaviors. The Landau expansion of the free-energy density F to describe the pressure- and the field-induced magnetic ordering for a spin-gap system is expressed as [27]

$$F = Am^2 + Bm^4 \quad (1)$$

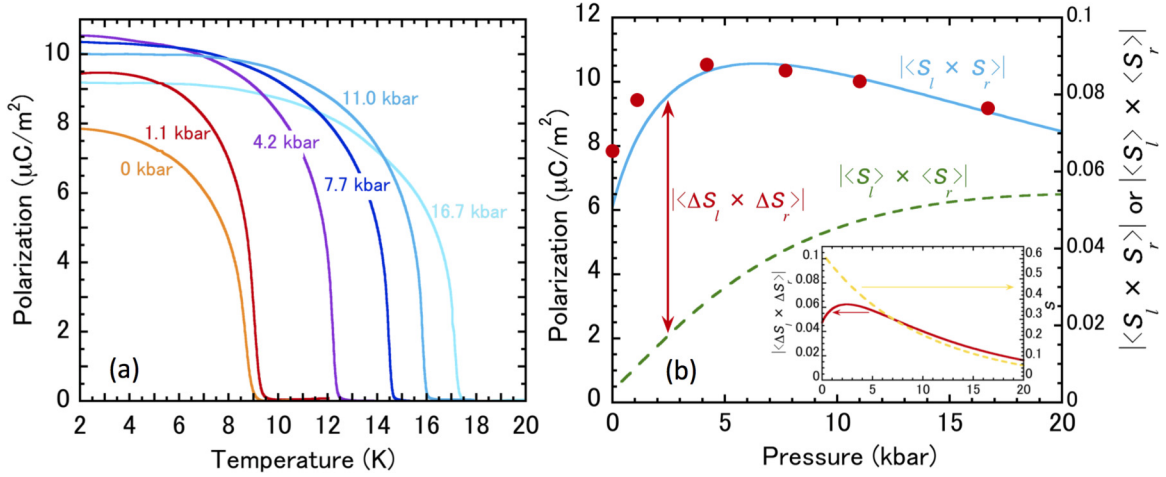


FIG. 2. (a) Temperature dependence of P (filled circles) under the applied pressure observed in TiCuCl_3 for $H \parallel [201]$ at 14 T. (b) Pressure dependence of P , observed in TiCuCl_3 for $H \parallel [201]$ at 14 T and 2 K. Solid and dashed curves denote the pressure dependencies of $|\langle S_l \times S_r \rangle|$ and $|\langle S_l \rangle \times \langle S_r \rangle|$, respectively, calculated based on the bond operator formulation. $|\langle \Delta S_l \times \Delta S_r \rangle|$ is given by the difference between $|\langle S_l \times S_r \rangle|$ and $|\langle S_l \rangle \times \langle S_r \rangle|$ as indicated by the double-headed arrow. The scale at the right side is for the values of $|\langle S_l \times S_r \rangle|$ and $|\langle S_l \rangle \times \langle S_r \rangle|$. The inset shows the calculated $|\langle \Delta S_l \times \Delta S_r \rangle|$ (solid curve) and the entanglement entropy s (dashed curve).

with

$$A = a_0 \left[1 + \left(\frac{T}{T_0} \right)^\phi - \left(\frac{H}{H_0} \right)^2 - \left(\frac{p}{p_0} \right) \right], \quad (2)$$

where \mathbf{m} is the staggered magnetic moment, and $a_0 > 0$ and $B > 0$ are constants. From previous magnetization measurements, the critical field H_0 at ambient pressure and the critical pressure p_0 at $H = 0$ T for the lowest temperature were determined to be $H_0 = 5.5$ T and $p_0 = 0.42$ kbar, respectively [18,26]. The phase boundary between the paramagnetic and magnetic ordered phases is given by the condition $A = 0$. As shown in Fig. 1(b), the theoretical curves calculated with $T_0 = 5.0$ K and $\phi = 3.0$ reproduce the experimental phase boundaries fairly well. The 3D exchange coupling between the dimers in TiCuCl_3 is considered to be a reason for the agreements between the theory and the experiment, because the Landau theory generally corresponds to a mean-field approximation. It should be noted that qualitatively the same pressure dependences of m and the critical field from the Landau theory are obtained from a bond operator formulation, which is based on a microscopic Hamiltonian, in the vicinity of p_0 when linear increases are assumed in the interdimer interactions with pressure [27,29]. Thus the pressure effects, demonstrated by the Landau theory, are interpreted to originate from the crossover to the classical 3D antiferromagnet due to the suppression of quantum spin fluctuation by pressure, as mentioned above. This result is consistent with previous neutron scattering measurements [25], which demonstrated an evolution of the magnetic ordered moment to $0.64\mu_B$ under pressure of 14.8 kbar at zero magnetic field, indicating that quantum fluctuation is considerably suppressed by pressure. Next, we discuss the pressure effects on spontaneous electric polarization P . Figure 2(a) shows the P - T curves under various values of pressure observed for $H \parallel [201]$ at 14 T. Development of P with cooling below the ordering temperature is observed. Figure 2(b) shows the pressure dependence of P at 2 K. The value of P initially increases as the pressure

is increased from the ambient pressure, while it saturates around 4 kbar and then gradually decreases in higher-pressure regions. At first glance, this decrease in P seems to contradict the stabilization of the magnetic order by pressure because P is generated by the appearance of finite vector spin chirality by the order. However, the observed behavior is consistently explained by the suppression of quantum fluctuation due to the application of pressure. As previously reported, P in TiCuCl_3 is proportional to the absolute value of $\langle S_l \times S_r \rangle$, which can be separated into two parts [15]:

$$P \propto |\langle S_l \times S_r \rangle| = |\langle S_l \rangle \times \langle S_r \rangle| + |\langle \Delta S_l \times \Delta S_r \rangle|, \quad (3)$$

with $\Delta S_i = S_i - \langle S_i \rangle$ ($i = l, r$). The first term on the right side denotes the contribution from the ordered components of the spins, whereas the second term denotes that from the quantum spin fluctuation. At ambient pressure, the contribution from the second term to P in TiCuCl_3 is significantly larger than that from the first term. According to the calculations in terms of the bond operator formulation for the ground state, more than 90% of the value of $\langle S_l \times S_r \rangle$ is attributed to the second term at ambient pressure at 14 T. As the pressure is increased, however, the contribution from the quantum fluctuation decreases, thereby resulting in a decrease in P in high-pressure regions. The pressure dependences of $|\langle S_l \times S_r \rangle|$ and $|\langle S_l \rangle \times \langle S_r \rangle|$, calculated in terms of bond operator formulation assuming the linear pressure dependences of the intra- and interdimer interactions, are shown in Fig. 2(b). The intradimer interaction $J(p) = J - ap$ and the interdimer interactions $\tilde{J}_k(p) = \tilde{J}_k + bp$ ($k = 1-3$) with $J = 5.5$ meV, $\tilde{J}_1 = 0.43$ meV, $\tilde{J}_2 = 3.16$ meV, $\tilde{J}_3 = 0.91$ meV, $a = 0.14$ meV/kbar, and $b = 0.075$ meV/kbar are used for the calculations. J and \tilde{J}_k were evaluated by analyzing the magnon dispersion, as tabulated in Refs. [29,30]; additionally, a and b were determined to reproduce $p_0 = 0.42$ kbar and the overall behavior of the pressure dependence of P . Although the ordered magnetic moments $0.94\mu_B$ at 14.8 kbar, calculated with the above parameters, are somewhat larger than the experimental value, evaluated from the neutron diffraction

measurement, the pressure dependence of P is found to be consistent with the calculated value of $|\langle \mathbf{S}_l \times \mathbf{S}_r \rangle|$, as shown by the solid curve in Fig. 2(b). As pressure is increased, the contribution from the ordered moments $|\langle \mathbf{S}_l \rangle \times \langle \mathbf{S}_r \rangle|$ monotonically increases due to the stabilization of the magnetic order, whereas $|\langle \mathbf{S}_l \times \mathbf{S}_r \rangle|$ decreases in high-pressure regions. This decrease occurs due to the suppression of the quantum fluctuation. Actually, the contribution from the quantum fluctuation $|\langle \Delta \mathbf{S}_l \times \Delta \mathbf{S}_r \rangle|$, which corresponds to the difference between $|\langle \mathbf{S}_l \times \mathbf{S}_r \rangle|$ and $|\langle \mathbf{S}_l \rangle \times \langle \mathbf{S}_r \rangle|$, decreases above 2.3 kbar as shown by the solid curve in the inset of Fig. 2(b), thereby decreasing the value of $|\langle \mathbf{S}_l \times \mathbf{S}_r \rangle|$ under high pressures. It is noteworthy that $\langle \Delta \mathbf{S}_l \times \Delta \mathbf{S}_r \rangle$ originates from quantum entanglement between the spins on the dimer because $\langle \Delta \mathbf{S}_l \times \Delta \mathbf{S}_r \rangle$ becomes finite only when the wave function Ψ of the spin dimer cannot be expressed by a direct product of the quantum states of two spins on a dimer. In the magnon BEC phase, Ψ is described by a coherent superposition of the spin-singlet and -triplet states as follows:

$$\Psi = C_1|0, 0\rangle + C_2|1, +1\rangle + C_3|1, -1\rangle \quad (4)$$

with $C_1 = u$, $C_2 = -vf$, and $C_3 = -vg$. Here, $|0, 0\rangle$ is the singlet state and $|1, \pm 1\rangle$ is the triplet state with the magnetic quantum number ± 1 of a dimer. u , v , f , and g are the real coefficients obtained from the bond operator formulation in Refs. [29,30]. Ψ is rewritten as $\Psi = \chi_i \tilde{C} \chi_r^T$ with

$$\chi_i = (|\uparrow\rangle_i, |\downarrow\rangle_i) \quad (5)$$

and

$$\tilde{C} = \begin{pmatrix} C_2 & C_1/\sqrt{2} \\ -C_1/\sqrt{2} & C_3 \end{pmatrix}, \quad (6)$$

where $|\uparrow\rangle_i$ and $|\downarrow\rangle_i$ denote the up and down spin states of \mathbf{S}_i ($i = l$ or r). The entanglement entropy s , which is a measure of the degree of quantum entanglement between two spins on a dimer in the quantum state Ψ , is given by

$$s = - \sum_{j=1}^2 q_j \ln q_j, \quad (7)$$

where q_j 's ($j = 1, 2$) denote the eigenvalues of the matrix $\tilde{C} \tilde{C}^T$. As shown in the inset of Fig. 2(b), s monotonically decreases as the pressure is increased because the system approaches a classical magnet. Our calculation demonstrates that $\langle \Delta \mathbf{S}_l \times \Delta \mathbf{S}_r \rangle$ decreases almost proportionally to s in the high-pressure regions. This suggests that the observed decrease in P occurs due to the unraveling of the quantum entanglement between the spins on a dimer upon the application of pressure. Our analyses also revealed that quantum entanglement significantly enhances the electric polarization in an interacting spin dimer system. It should be mentioned that the application of pressure monotonically decreases the entanglement entropy s , while $\langle \Delta \mathbf{S}_l \times \Delta \mathbf{S}_r \rangle$ is increased by pressure below 3 kbar as shown in the inset in Fig. 2(b). The reason for this difference in the behaviors between s and $\langle \Delta \mathbf{S}_l \times \Delta \mathbf{S}_r \rangle$ can be explained as follows. The quantum state of a spin dimer with the largest s is the spin-singlet state. At ambient pressure, the wave function in the ground state of a dimer in TiCuCl_3 at 14 T is mainly composed of this singlet state, and the spin-triplet components, induced by the magnetic field, also

contribute slightly to the ground state. By the application of pressure, the ratio of the spin-triplet components contributing to the ground state is increased, while that of the singlet state is decreased. This change in the ground-state wave function due to pressure causes the monotonic decrease in s and a crossover to a classical spin flop state. On the other hand, because the spin-singlet state has no finite $\langle \Delta \mathbf{S}_l \times \Delta \mathbf{S}_r \rangle$, the participation of the triplet states to the ground state is required for finite $\langle \Delta \mathbf{S}_l \times \Delta \mathbf{S}_r \rangle$. Thus, $\langle \Delta \mathbf{S}_l \times \Delta \mathbf{S}_r \rangle$ gradually increases as the pressure is increased in the low-pressure region, in contrast to s . However, because $\langle \Delta \mathbf{S}_l \times \Delta \mathbf{S}_r \rangle$ becomes zero for a classical spin state without quantum fluctuation, $\langle \Delta \mathbf{S}_l \times \Delta \mathbf{S}_r \rangle$ decreases in the high-pressure region. This is the reason for the peak of $\langle \Delta \mathbf{S}_l \times \Delta \mathbf{S}_r \rangle$ seen in the inset in Fig. 2(b).

Finally, we show the pressure dependence of the P - E hysteresis. As mentioned above, the ferroelectricity in TiCuCl_3 is very soft [16]. P in TiCuCl_3 can be reversed by low electric fields $E_r \simeq 0.03$ MV/m at ambient pressure. However, under applied pressure, the ferroelectricity becomes harder, as shown in Fig. 3(a). The width of the P - E hysteresis loop observed at 4.2 K and 14 T for $H \parallel [201]$ largely increases as the pressure is increased. The pressure dependence of the electrostatic energy PE_r , required for the reversal of P , is plotted in Fig. 3(b). PE_r increases almost linearly with pressure. Here, because it is difficult to obtain a precise value of P from the P - E hysteresis measurement, P at 4.2 K, obtained from the P - T curves, is used to calculate PE_r . The mean value of the cohesive fields E_r between up and down processes in the E -field is also used. The reversal of P requires the antiferromagnetic domain to be rotated by 180° , which rotates the vector spin chirality. Thus, an inevitable magnetic anisotropy around the external magnetic field, which forces the staggered magnetic ordered moment \mathbf{m} to be aligned along a direction with the lowest anisotropy energy, becomes the origin of the finite E_r , because it tends to prevent the rotation of \mathbf{m} . This situation can be described using the Landau free energy by adding an anisotropy in the xy -plane where the \mathbf{m} lies, as follows [31]:

$$F = A\mathbf{m}^2 + B\mathbf{m}^4 - 2\gamma m^2 \cos 2\theta. \quad (8)$$

Here, the last term represents the anisotropy with an angle θ between \mathbf{m} and the magnetic easy x -axis and a positive constant γ . As illustrated in the inset of Fig. 3(b), anisotropy gives rise to two potential minima on the potential surface of F/B along with potential barriers at the saddle points between the minima. The 180° rotation of the antiferromagnetic domain corresponds to the rotation of \mathbf{m} from the direction of one of the two minima to the other. Thus, to rotate the magnetic domain, the potential barrier should be passed over by applying an electric field, thereby resulting in finite E_r . From the Landau free energy in Eq. (8), the height of the potential barrier ΔU is given by

$$\Delta U = -\frac{2\gamma A}{B} = \frac{2\gamma a_0}{B} \left[-1 - \left(\frac{T}{T_0} \right)^\phi + \left(\frac{H}{H_0} \right)^2 + \left(\frac{p}{p_0} \right) \right]. \quad (9)$$

Thus, the Landau theory indicates that ΔU linearly increases with pressure as seen for PE_r . ΔU , calculated by substituting $2\gamma a_0/B = 0.0225$ J/m² and other parameters noted above

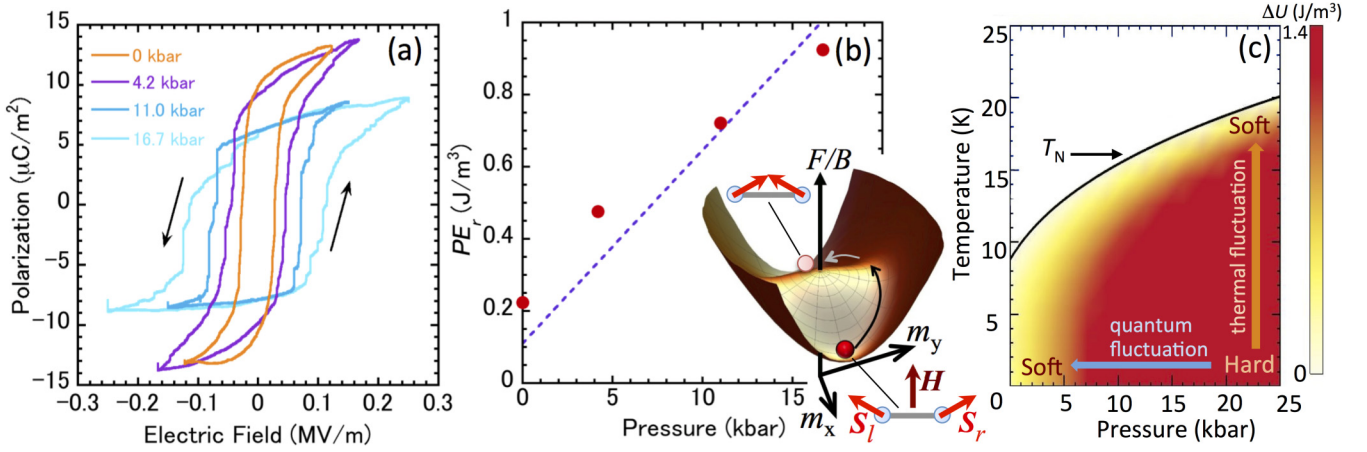


FIG. 3. (a) P - E hysteresis loops observed in TiCuCl_3 for $H \parallel [201]$ at 14 T and 4.2 K under the applied pressure. (b) Pressure dependence of PE_r , observed in TiCuCl_3 at 14 T and 4.2 K (filled circles). The dashed line is calculated on the basis of the Landau theory. The inset shows the potential surface calculated from Eq. (8). (c) Contour plot of the potential barrier ΔU . Solid curve shows a phase boundary between the disordered and ordered phases.

into Eq. (9), was found to be consistent with the pressure dependence of the experimental PE_r , as shown in Fig. 3(b). This consistency suggests that PE_r increases due to an increase in ΔU when pressure is applied. Because ΔU originates from the anisotropy, which is proportional to m^2 in Eq. (8), the stabilization of the magnetic order upon the application of pressure is considered to cause the hardening of P . Pressure and temperature dependences of ΔU , shown in Fig. 3(c), suggest that in low-temperature and high-pressure regions with a high value of ΔU , P is hard due to the stabilization of the order. Then, the ferroelectricity becomes soft with warming due to activation of the thermal fluctuation; meanwhile, softening also occurs due to the activation of quantum fluctuation when the pressure is decreased. As shown in Fig. 4(a), PE_r , observed at 14 T at ambient pressure, decreases with warming, and then approaches zero at the

transition temperature around 8 K as shown in Fig. 4(a). A decrease in PE_r with decreasing magnetic field is also observed. As shown in Fig. 4(b), PE_r at 1.7 K at ambient temperature approaches zero at the critical field around 5.5 T as expected from the Landau theory. The above results indicate that the stiffness of ferroelectricity in TiCuCl_3 can be controlled by tuning the strength of the quantum fluctuation with the application of pressure. It is also indicated that the quantum fluctuation plays a key role in yielding the soft nature of the ferroelectricity.

IV. SUMMARY

To summarize, with high-pressure measurements we demonstrated a large change in the phase boundary curve in the temperature-field phase diagram of TiCuCl_3 due to the suppression of quantum spin fluctuation by pressure. We also

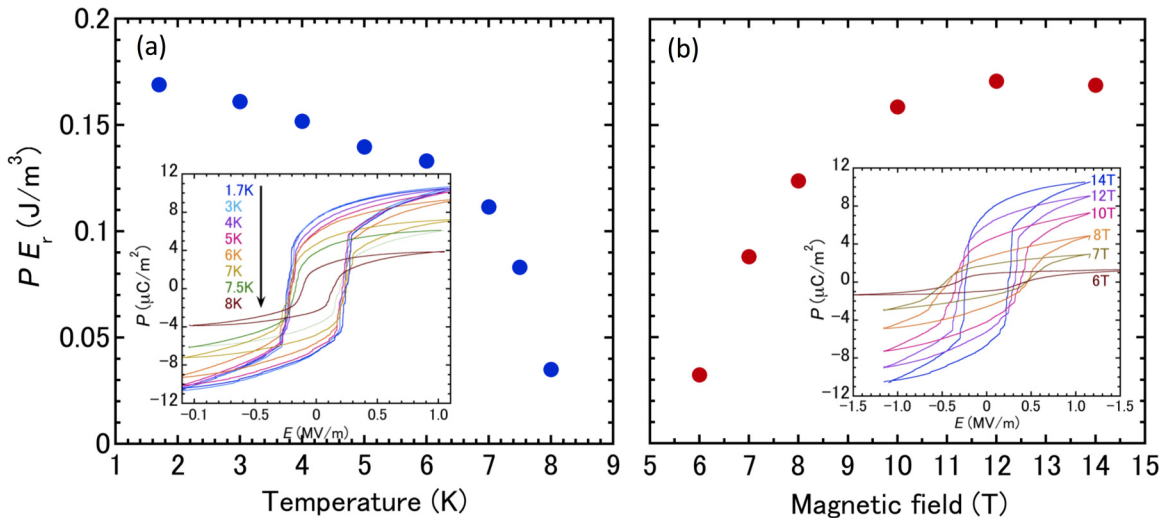


FIG. 4. (a) Temperature dependence of PE_r , observed in TiCuCl_3 for $H \parallel [201]$ at 14 T at ambient pressure. The inset shows the temperature dependence of P - E hysteresis loop. (b) Magnetic field dependence of PE_r , observed in TiCuCl_3 for $H \parallel [201]$ at 1.7 K at ambient pressure. The inset shows the magnetic field dependence of P - E hysteresis loop.

revealed that the application of pressure, which causes the crossover of the spin Hamiltonian to a 3D system, unravels the quantum entanglement between the degrees of freedom of the two spins on a dimer, resulting in decreased electric polarization. Furthermore, it was found that the stiffness of ferroelectric polarization in TiCuCl_3 can be controlled by tuning the strength of the quantum fluctuation with pressure. Our results indicated that quantum fluctuation makes decisive contributions in the determination of the nature of spin-driven ferroelectricity in quantum magnets.

ACKNOWLEDGMENTS

The authors are grateful to T. Sakurai and H. Okada for their advice on the high-pressure experiments, and to K. Okunshi for valuable discussions. This work was partly supported by Grants-in-Aid for Scientific Research (Grants No. 17H01142, No. 17H02917, No. 17K05516, and No. 19H01834) from MEXT Japan. This work was performed at the High Field Laboratory for Superconducting Materials, Institute for Materials Research, Tohoku University (Project No. 17H0412).

-
- [1] T. Kimura, T. Goto, H. Shintani, K. Ishizaka, T. Arima, and T. Tokura, *Nature (London)* **426**, 55 (2003).
- [2] S.-W. Cheong and M. Mostovoy, *Nat. Mater.* **6**, 13 (2007).
- [3] T. Arima, *J. Phys. Soc. Jpn.* **80**, 052001 (2011).
- [4] T. Tokura, S. Seki, and N. Nagaosa, *Rep. Prog. Phys.* **77**, 076501 (2014).
- [5] T. Moriya, *J. Appl. Phys.* **39**, 1042 (1968).
- [6] M. Matsumoto, K. Chimata, and M. Koga, *J. Phys. Soc. Jpn.* **86**, 034704 (2017).
- [7] H. Katsura, N. Nagaosa, and A. V. Balatsky, *Phys. Rev. Lett.* **95**, 057205 (2005).
- [8] M. Mostovoy, *Phys. Rev. Lett.* **96**, 067601 (2006).
- [9] I. A. Sergienko and E. Dagotto, *Phys. Rev. B* **73**, 094434 (2006).
- [10] C. Jia, S. Onoda, N. Nagaosa, and J. H. Han, *Phys. Rev. B* **76**, 144424 (2007).
- [11] T. A. Kaplan and S. D. Mahanti, *Phys. Rev. B* **83**, 174432 (2011).
- [12] K. Kimura, Y. Kato, K. Yamauchi, A. Miyake, M. Tokunaga, A. Matsuo, K. Kindo, M. Akaki, M. Hagiwara, S. Kimura, M. Toyoda, Y. Motome, and T. Kimura, *Phys. Rev. Mater.* **2**, 104415 (2018).
- [13] Y. Kato, K. Kimura, A. Miyake, M. Tokunaga, A. Matsuo, K. Kindo, M. Akaki, M. Hagiwara, S. Kimura, T. Kimura, and Y. Motome, *Phys. Rev. B* **99**, 024415 (2019).
- [14] S. Kimura, K. Kakihata, Y. Sawada, K. Watanabe, M. Matsumoto, M. Hagiwara, and H. Tanaka, *Nat. Commun.* **7**, 12822 (2016).
- [15] S. Kimura, K. Kakihata, Y. Sawada, K. Watanabe, M. Matsumoto, M. Hagiwara, and H. Tanaka, *Phys. Rev. B* **95**, 184420 (2017).
- [16] S. Kimura, M. Matsumoto, and H. Tanaka, *Phys. Rev. Lett.* **124**, 217401 (2020).
- [17] K. Takatsu, K. Shiramura, and H. Tanaka, *J. Phys. Soc. Jpn.* **66**, 1611 (1997).
- [18] W. Shiramura, K. Takatsu, H. Tanaka, K. Kamishima, M. Takahashi, H. Mitamura, and T. Goto, *J. Phys. Soc. Jpn.* **66**, 1900 (1997).
- [19] T. Nikuni, M. Oshikawa, A. Oosawa, and H. Tanaka, *Phys. Rev. Lett.* **84**, 5868 (2000).
- [20] G. Misguich and M. Oshikawa, *J. Phys. Soc. Jpn.* **73**, 3429 (2004).
- [21] F. Yamada, T. Ono, H. Tanaka, G. Misguichi, M. Oshikawa, and T. Sakakibara, *J. Phys. Soc. Jpn.* **77**, 013701 (2008).
- [22] T. Giamarchi, T. Rüegg, and O. Tchernyshyov, *Nat. Phys.* **4**, 198 (2008).
- [23] V. Zapf, M. Jaime, and C. D. Batista, *Rev. Mod. Phys.* **86**, 563 (2014).
- [24] H. Tanaka, A. Oosawa, T. Kato, H. Uekusa, Y. Ohashi, K. Kakurai, and A. Hoser, *J. Phys. Soc. Jpn.* **70**, 939 (2001).
- [25] A. Oosawa, M. Fujisawa, T. Osakabe, K. Kakurai, and H. Tanaka, *J. Phys. Soc. Jpn.* **72**, 1026 (2003).
- [26] K. Goto, M. Fujisawa, T. Ono, H. Tanaka, and Y. Uwatoko, *J. Phys. Soc. Jpn.* **73**, 3254 (2004).
- [27] M. Matsumoto and M. Sigrist, *J. Phys. Soc. Jpn.* **74**, 2310 (2005).
- [28] H. D. Scammell and O. P. Sushkov, *Phys. Rev. B* **95**, 094410 (2017).
- [29] M. Matsumoto, B. Normand, T. M. Rice, and M. Sigrist, *Phys. Rev. B* **69**, 054423 (2004).
- [30] M. Matsumoto, B. Normand, T. M. Rice, and M. Sigrist, *Phys. Rev. Lett.* **89**, 077203 (2002).
- [31] R. Dell'Amore, A. Schilling, and K. Krämer, *Phys. Rev. B* **79**, 014438 (2009).